



An Analytical Model for Fluid Imbibition in Organic Nanopores

Shu Yang¹

Received: 29 June 2018 / Accepted: 23 October 2019 / Published online: 2 November 2019
© Springer Nature B.V. 2019

Abstract

Estimating the fluid imbibition flow in natural system composed of nanopores is challenging due to the strong fluid/rock molecular scale interaction and the invalidation of the macroscopic thermodynamics treatment. We develop an analytical model for Lennard-Jones fluid imbibition into an organic nanopore considering the phase transition and fluid/rock intermolecular interactions. In addition, we apply the proposed model on octane molecules imbibition into 1–10 nm slit-shape graphite nanopores under the standard and shale reservoir condition. Predicted velocity and density profiles of 2 nm model at the standard condition show that octane molecules first imbibe as vapor phase at around 200–300 m/s and form adsorbed layers near the pore wall. Velocity and density profiles are compared with the molecular dynamic simulation results. Calculated mean velocities of the analytical model and simulation are around 10^3 – 10^4 of those predicted by classical models, which are similar with previous experimental results. Reservoir condition results show octane can fast flow only when the driving pressure is greater than 0.12 MPa when the initial reservoir pressure is 5.72 MPa. Particularly, the impact of the fluid phase transition on the imbibition rate is significant in organic nanopores.

Keywords Imbibition · Adsorption · Nanopore · Phase transition

1 Introduction

As the arising development of organic-rich tight and shale reservoirs, which consist of organic nanopores, the estimation of hydrocarbon stored and recoverable oil in organic nanopores are significant for oil industries (Lan et al. 2015). Organic nanopores is one of three main pore spaces where hydrocarbon is mainly stored in organic-rich tight and shale reservoirs (Riewchotisakul and Akkutlu 2016). The key factor of recoverable reserve estimation is to investigate the transport of oil in nanopores.

In addition, the fluid flow mechanism in nanopores is very different with the classical continuum model (Cai et al. 2014; Cai and Yu 2011; Saif et al. 2016). For nature shale and tight rocks, which are organic-rich and composed of nanopores, recent contact angle tests

✉ Shu Yang
yangshuwalcf@126.com

¹ EOR Center, SINOPEC Exploration and Production Research Institute, Beijing 100083, China

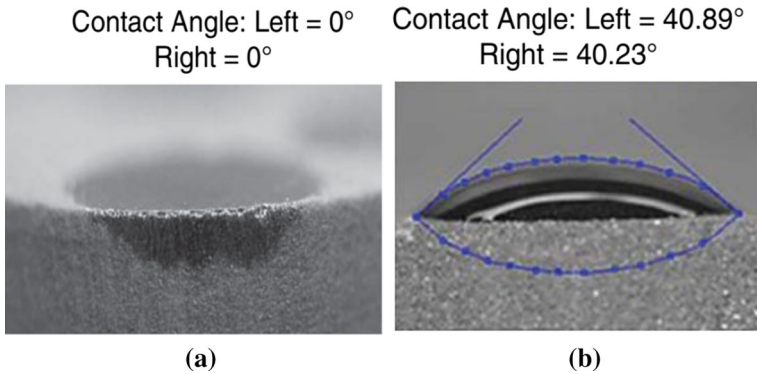


Fig. 1 Contact angles of oil (a) and brine (b) on the dry and clean surface of tight rock samples (Lan et al. 2015)

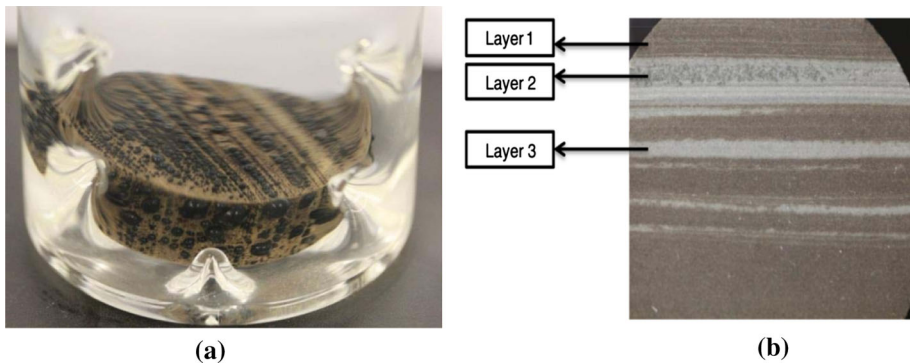


Fig. 2 a Saturated oil samples in the brine (Habibi et al. 2016) and b cross section of the target sample (Habibi et al. 2016). In b, Layer 1 contains more quartz and feldspars, Layer 2 contains more pyrite, quartz and feldspars and Layer 3 contains more quartz, feldspars and carbonates

(Lan et al. 2015) (Fig. 1) showed that oil with less capillary pressure could imbibe into tight rocks immediately. These results indicate the classical theory cannot explain the previous contact angle result. Yassin et al. (2016) measured the oil fast imbibition and Habibi et al. (2016) conducted counter-current imbibition at room pressure and temperature. Their results (Yassin et al. 2016) showed oil could fast imbibition into organic nanopores. Therefore, it is essential for investigating the fluid imbibition flow in nanopores (Fig. 2).

Recent researches (Supple and Quirke 2004, 2005; Wang et al. 2016; Whitby and Quirke 2007; Gruener et al. 2009; Sokhan et al. 2001) on fluid transports in nanopores mainly focus on simulations and experiments. Current analytical studies generally use equations of Young and Laplace (YL) (Rowlinson and Widom 1982) and Hagen–Poiseuille (HP) model to calculate the driving pressure and the velocity at macroscale, respectively. Particularly, recent theoretical and experimental researches presented the fluid surface tension at nanoscale is significantly different with the bulk value (Supple and Quirke 2004) and is hard to measure. In addition, it is challenging to analytically model the fluid flow in nanopores due to the invalidation of macroscopic thermodynamics treatment at molecular scale (pore size ≤ 8 nm) (Supple and Quirke 2004, 2005; Wang et al. 2016), the complex phase transition (Whitby and Quirke 2007) and the lack of accessible driving pressure and motion equation. There is a

need for further analytical model of the fluid imbibition in organic nanopores meeting above challenges.

Supple and Quirke (Supple and Quirke 2004, 2005) simulated decane molecules imbibition in 0.7–2.2 nm carbon nanotubes using molecular dynamic method. Their simulation results presented the surface tension of decane molecules in nanopores ranges from 0.8 to 9.87 mN/m, which is significantly less than bulk value (22–23 mN/m). Imbibition rates of decane molecules in 1.3–2.2 nm carbon nanotube range from 10 to 400 m/s, which are 10^2 – 10^4 of imbibition rate expected by classical models. These results suggest the driving pressure of fluid imbibition in nanopores cannot be calculated by the bulk surface tension and the fluid flow rate is extremely high. Rossi and Ye (2004) conducted experiments to investigate water condensation in a 50–250 nm carbon nanotube. The temperature of the set-up was set constant, generally to 4 or 5 °C. Their transmission electron microscopy (TEM) images of water meniscus in a carbon nanotube indicated the condensation phenomenon. Their visualized video results showed the existent of the phase transition during the flow procedure. These results indicate classical models, ignoring phase transition, cannot describe the fluid imbibition in nanopores. Jin and Firoozabadi (2015) investigated the phase behavior and pressure-driven flow of methane in carbon slits using density functional theory and molecular dynamic simulations. They showed the flux is around one to two orders of magnitude larger than predictions from the Knudsen diffusion and HP equation in 3 nm long carbon nanopores. In addition, Majumder et al. (2005a) measured the pressure-driven flow of hexane and decane through around 7 nm carbon nanotube membranes at 0.7–1 bar applied pressure. All experiment set-ups were placed at the room temperature during the whole procedure. Carbon nanotube membranes were initially dry in the air, and then, place is the sealed flow cell at 1.01 bar before experiments. Measured flow rates of hexane and decane are around 10^4 and 10^3 of those predicted by the classical model, respectively. This result indicates that the fluid flow in organic nanopores is significantly faster than that expected by classical models.

In this paper, we develop an analytical model for a Lennard-Jones (LJ) fluid imbibition into organic nanopores, which considers the phase transition, the fluid/wall intermolecular interaction and the invalidation of macroscopic thermodynamics treatment. The objective of this paper is to investigate phase transition, adsorption and imbibition rates in organic nanopores. The rest of this paper is composed of following sections. In Sect. 2, we develop an analytical model for LJ fluid imbibition in 1–10 nm organic nanopores using density functional theory (DFT) (Tarazona 1985; Lastoskie et al. 1993; Li et al. 2014), local chemical potential differences and Newton's law. In Sect. 3, we simulate octane molecules imbibition into 1–10 nm graphite slits to compare with analytical model results. In Sect. 4, we apply the proposed model on octane molecules imbibition into 1–10 nm graphite slit-shape pores under standard condition and reservoir condition. In Sect. 5, we discuss the limitation and the inaccuracy of the proposed model.

2 Theoretical Models

In this paper, we model the LJ fluid imbibition in organic nanopores using analytical model and molecular dynamic (MD) simulation. Both the analytical model and the MD simulation use the same imbibition model, which is schematically illustrated in Fig. 3. The open-end slit represents the organic nanopore, which is composed of two gray graphite substrates. The slit is initially dry, and then placed in a fluid reservoir filled with the bulk fluid. From the contact angle and imbibition experiments, we know the wettability of rocks is measured

Fig. 3 Schematic illustration of the imbibition model. The green and the gray parts represent the fluid molecules and the slit, respectively. The width, length and depth of the slit are denoted by w , L and h , respectively. The distance from the slit center is x , and the imbibed length is l

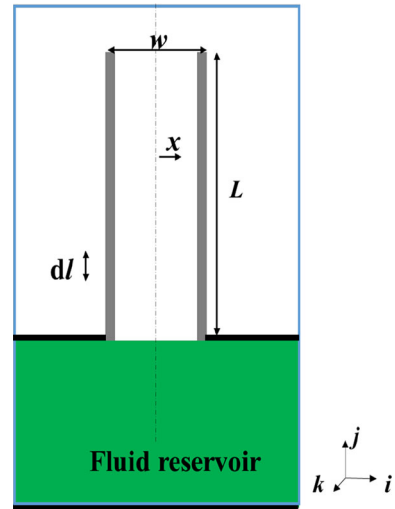


Table 1 Comparison of gravities and surface tension calculated by YL equation of fluid molecules in different size nanopores

Condition	$T = 300 \text{ K}, P = 0.1 \text{ MPa}$				$T = 353 \text{ K}, P = 23.47 \text{ MPa}$			
Width (nm)	1	2	5	10	1	2	5	10
Density (g cm^{-3})	0.89	0.81	0.78	0.75	1.18	1.04	0.89	0.81
Gravity (10^{-20} N)	0.13	0.24	0.57	1.10	0.17	0.30	0.65	1.20
Surface tension _{YL} (10^{-9} N)	6.6	3.3	1.32	0.66	6.6	3.3	1.32	0.66

at the standard condition. Thus, the temperature, T , and pressure, P of the system are set to 298 K and 0.1 MPa, respectively. Combined with the pore size distribution analysis of previous target organic-rich shale (Lan et al. 2015), we select 1–10 nm organic pores. Thus, open-end nanopores, ranging from 1 to 10 nm, are the vacuum before the imbibition under the condition of room temperature and pressure. According to the comparison with the surface tension calculated by YL equation (Table 1), the gravity of fluid molecules at nanoscale is extremely small and can be neglected, as similarly done (Supple and Quirke 2004, 2005; Wang et al. 2016; Lastoskie et al. 1993; Li et al. 2014; Ravikovitch et al. 2001).

2.1 Density Model

According to previous studies (Tarazona 1985; Lastoskie et al. 1993; Li et al. 2014; Ravikovitch et al. 2001), phase behaviors of fluid in nanopores are complex and fluid molecule distribution at the cross section of the nanopores is inhomogeneous. Considering fluid density oscillation in the nanopore and phase transition, non-local DFT is used to model the fluid density profile. Non-local DFT has successfully applied to investigate the condensation profile and phase transition in previous studies (Tarazona 1985; Lastoskie et al. 1993; Li et al. 2014; Ravikovitch et al. 2001). Since non-local DFT is used to model the LJ fluid (Tarazona

1985), we choose LJ fluid in the proposed model. In addition, the fluid molecule is modeled by the hard-sphere method (Tarazona 1985).

Assumptions of the proposed model are listed as:

- a. The system is *NVT* system. Temperature of the whole system and the pressure of the fluid reservoir are constant.
- b. Single-phase fluid molecules imbibe into the slit.
- c. Fluid density distributions are homogeneous within dl along j -axis. We divide the slit length into various dl (j -axis): $L = \int_0^L dl$. Within each dl , we assume the fluid density distribution along j -axis is homogeneous. For different dl , the fluid density distribution along j -axis is different.
- d. The imbibition time is at pico second scale. According to our and previous MD simulation works (Supple and Quirke 2004, 2005; Jin and Firoozabadi 2015, 2016), the fluid flow rate is relatively steady within several ps. Thus, the time interval of the proposed model is at ps scale.

Then, the density profile of fluid molecules on the cross section of the nanopore at dl can be calculated by (Tarazona 1985; Lastoskie et al. 1993; Li et al. 2014; Ravikovitch et al. 2001)

$$\ln \rho(x) = \frac{1}{kT} \left(-\mu + V_{\text{ext}}(x) + f_{\text{ex}}(\bar{\rho}(x)) + \int_V x' \rho \Phi_{\text{att}}(|x - x'|) dx' - kT \int_V \lambda(x') w_i[|x - x'|; \bar{\rho}(x')] dx' \right) - \ln \Lambda^3 \tag{1}$$

$$\lambda(x) = \frac{-\rho(x) f'_{\text{ex}}(\bar{\rho}(x)) / kT}{\left[1 - \int_V \frac{\partial w_i[|x - x'|; \bar{\rho}(x)]}{\partial \bar{\rho}(x)} \rho(x') dx' \right]} \tag{2}$$

where $V_{\text{ext}}(x)$, Φ_{att} and $\bar{\rho}(x)$ are the external potential of fluid molecules, the fluid/fluid van der Waals attraction potentials and the smoothed density, respectively. x and x' are the distance from the slit center, respectively. $f_{\text{ex}}[\rho(x); d]$, w_i and μ are the excess hard-sphere Helmholtz free energy, the normalized weight function (Tarazona 1985) and chemical potential of the bulk fluid, respectively. Details of DFT are presented in “Appendix A.”

2.2 Driving Pressure

Generally, the thickness of fluid in the interfacial tension test is around 10^{-3} m. At this scale, the fluid is a continuum and single-phase fluid, which is very different with fluid at nanoscale. According to previous studies (Supple and Quirke 2004, 2005), fluid molecules in the nanopore are not continuum fluid. An accurate experimental measurement of the surface tension of fluid in the nanopores is not easy (Ravikovitch et al. 2001). Previous study (Zeng et al. 2011) has shown the line tension difference can be calculated as the driving pressure at nanoscale. Considering the line tension, which is the excess free energy per unit length of the line where two phases meet (Zeng et al. 2011), and the fluid/pore intermolecular interactions, we calculate the chemical potential difference, $\Delta\mu$, between fluid in the nanopore and bulk fluid as the driving pressure of the imbibition. According to statistical mechanics (Hummer

et al. 1996; Qin et al. 2011), the average number of fluid molecules ($\langle N \rangle$) of a specific volume at dl is related to the local excess chemical potential difference as (Hummer et al. 1996)

$$\frac{N}{\rho_{\text{bulk}} \Delta V} = \exp \left[-\frac{1}{kT} (\mu_{\text{in}}^{\text{ex}} - \mu_{\text{bulk}}^{\text{ex}}) \right] = \exp \left(-\frac{1}{kT} \Delta \mu \right) \quad (3)$$

where ρ_{bulk} and ΔV are the bulk fluid density and the specific volume at the cross section of the nanopore at dl , respectively. $\mu_{\text{in}}^{\text{ex}}$ and $\mu_{\text{bulk}}^{\text{ex}}$ are the fluid molecules inside the nanopore and the bulk fluid, respectively.

The chemical potential difference can be calculated by (Qin et al. 2011)

$$\Delta \mu = RT \ln \frac{\rho_{\text{bulk}}}{\rho} \quad (4)$$

where R and ρ are gas constant and density of fluid molecules at equilibrium state in the nanopore, respectively. The driving pressure, ΔP , is determined by the chemical potential difference (Qin et al. 2011):

$$\Delta P = -\frac{\Delta \mu}{V_{\text{mol}}} = -\frac{RT}{V_{\text{mol}}} \ln \frac{\rho_{\text{bulk}}}{\rho(x)} \quad (5)$$

where V_{mol} is the molar volume of fluid. Since the density is a function of x , the driving pressure can be calculated as a function of x . Pressure is a basic thermodynamic variable that defines the state of a system and can be defined at nanoscale (McQuarrie 1976). To connect the chemical potential difference and the driving force, pressure is defined as the force per unit area in the proposed model, which is similar with previous work (McQuarrie 1976). Combined with assumption c, we define fluid density at dl as ρ_t and ρ_{t-1} are the imbibed fluid density at dl of specific time step t and that of one-time step before t , respectively. Then, the driving pressure can relate to the chemical potential difference in Eq. 5. In the proposed model, the driving pressure of specific time, t at dl is calculated as

$$\Delta P_t(x) = -\frac{RT}{V_{\text{mol}}} \ln \frac{\rho_{t-1}(x)}{\rho_t(x)} \quad (6)$$

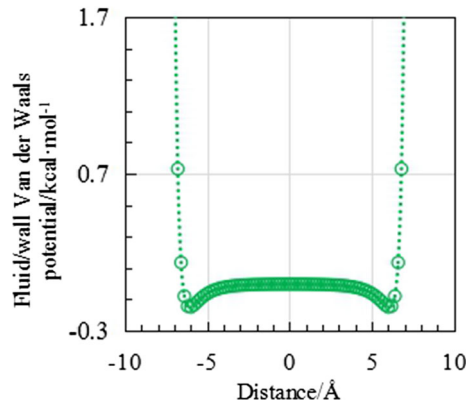
Here ΔV of Eq. 3 is defined as the volume, the width of which is x at the cross section along i -axis, the depth of which is 5 nm along k -axis and the length of which is dl along j -axis. Thus, $\rho_t(x)$ and $\rho_{t-1}(x)$ of Eq. 6 are related to Eqs. 1–2. Values of $\rho_t(x)$ and $\rho_{t-1}(x)$ in Eq. 6 are discussed in Sect. 5.

2.3 Imbibition Model

According to previous work (Whitby and Quirke 2007) and our results, fluid pressure within a 50–10² nm distance along j -axis is orders of magnitude variations. In this paper, dl is set to be 3 nm and discussed in Sect. 5. In addition, the time scale of the proposed model should be peso second to keep the pressure variation steady. According to previous experimental works (Whitby and Quirke 2007; Wang et al. 2014) and simulation works (Supple and Quirke 2004, 2005; Ravikovitch et al. 2001), fluid pressure and density at peso second scale within 3 nm distance interval along j -axis are relatively steady.

Considering the macroscopic thermodynamics' treatment fails in continuous region (<8 nm) (Liu and Li 2011) and the equilibrium distance between fluid and wall, we apply

Fig. 4 Fluid/wall van der Waals potentials of imbibed octane molecules versus distances from the slit center in 2 nm model



Newton’s law on fluid molecules in 1–10 nm models. The total force, F , applied on all fluid molecules at distance x can be calculated by

$$F = m(x) \frac{dv(x)}{dt} \tag{7}$$

where m and v are the mass and the velocity of fluid molecules at t , respectively.

The driving force, F_d , is

$$F_d = \Delta P(x) \cdot h \cdot dx \tag{8}$$

In this paper, the force of the fluid/wall interaction is quantitatively described by the mean ‘friction’ force, F_i , and the ‘collision coefficient,’ α^{10} . Due to the fluid/wall intermolecular attractive energy, fluid molecules will move toward the wall. When the distance between the fluid molecule and the wall atom is less than the equilibrium distance (Eq. A9), the fluid/wall attractive energy turns to be repulsive energy. Thus, the fluid molecule velocity along i -axis toward the wall decreases, and then the velocity away from the wall increases. This procedure is macroscopically defined as the collision. In fact, the fluid molecule does not collide with the wall. For instance, we calculate the fluid of octane molecules in 2 nm graphite slit. Figure 4 shows the fluid/wall van der Waals potential of imbibed octane molecules in 2 nm nanopore. The impact of the fluid/wall intermolecular interaction is significantly obvious near the wall. The thickness of such impact region, h_{ads} is around $2\sigma_{sf}$ for 2 nm model. The impact of the fluid/wall interaction is relatively weak in the center region, and the thickness of the center region is $(w - 2h_{ads})$. Therefore, mean ‘friction’ force and α are defined within the impact region.

For the impact region, where $-w/2 < -x < -w/2 + h_{ads}$ and $w/2 - h_{ads} < x < w/2$, the impact of the fluid/wall interaction are quantitatively calculated as (Tarazona 1985)

$$\alpha = \frac{u_{out} - u_{in}}{v(x)} \tag{9}$$

where u_{in} and u_{out} are the velocity of fluid molecules near the wall before and after the fluid/wall interaction, respectively. Since α is caused by the fluid/wall van der Waals interactions, $\alpha = 0$ in the center region when $-w/2 + h_{ads} < x < w/2 - h_{ads}$.

Then, F_i can be calculated as

$$F_i = \alpha m(x)v(x) \tag{10}$$

Table 2 Parameters of intermolecular interactions used in analytical models (Tarazona 1985; Lastoskie et al. 1993; Li et al. 2014; Ravikovitch et al. 2001)

T (K)	k (10^{-23} J/K)	Λ (Å)	ϵ_{ff} (kcal/mol)	σ_{ff} (Å)	ϵ_{sf} (kcal/mol)	σ_{sf} (Å)	α
298	1.38	0.87	0.10	3.8	0.15	3.5	0.002

Combing Eqs. 7–10, we get

$$F = (F_d - F_i) = \Delta P(x) \cdot h \cdot dx - \alpha m(x)v(x) = m(x) \frac{dv(x)}{dt} \quad (11)$$

Since $m(x) = dx \cdot l \cdot h \cdot \rho(x)$ and $dv = dl/dt$, we have

$$\frac{d^2[l^2(x)]}{dt^2} + \alpha \frac{d[l^2(x)]}{dt} = \frac{2\Delta P(x)}{\rho(x)} \quad (12)$$

For $-w/2 < -x < -w/2 + h_{ads}$ and $w/2 - h_{ads} < x < w/2$, we get

$$v(x) = \frac{1}{2} \cdot \left(\frac{2\Delta P(x)}{\rho_t(x)} \right)^{1/2} (1 - e^{-\alpha t})(\alpha t + e^{-\alpha t} - 1)^{-1/2} \quad (13)$$

For $-w/2 + h_{ads} < x < w/2 - h_{ads}$, we get

$$v(x) = \left(\frac{-RT \ln \frac{\rho_{t-1}(x)}{\rho_t(x)}}{V_{mol} \rho_t(x)} \cdot e^t \right)^{1/2} \quad (14)$$

According to assumption d, the time scale is ps, which means e^t is around 1. In the proposed model, fluid molecules move toward both i -axis, j -axis and k -axis. Since there is no pore wall along k -axis, fluid molecule distribution is homogeneous. Since two pore walls along i -axis are the same, fluid molecule distribution and velocity are symmetric.

In this paper, we apply the proposed model on octane molecules in 1–10 nm graphite slit. Table 2 lists parameters used in the analytical model (Eqs. A6–A9). In the proposed analytical model, σ_{ff} and σ_{sf} are the equilibrium distance between octane/octane and octane/graphite molecules, respectively. ϵ_{ff} and ϵ_{sf} are potential well of the van der Waals energy between octane/octane and octane/graphite molecules, respectively. Subscripts of f and s represent the fluid and wall.

3 Molecular Dynamic Simulation

To investigate details of the phase behavior and fluid transport, we previously performed the MD simulation (Yang et al. 2016) of octane molecules imbibition into 1–10 nm graphite nanopores using Material Studio 7.0 (Run by Shenzhen cloud computing center of the China national supercomputing center in Shenzhen). The MD simulation model is the same as the analytical model and illustrated in Fig. 3. The size of the simulation cell and fluid reservoir are $100 \times 50 \times 5$ nm and is $100 \times 20 \times 5$ nm, respectively. L and h of the simulation model are 30 nm and 5 nm, similarly done (Supple and Quirke 2004, 2005). Bulk density of octane molecule reservoir is set to 0.74 g/cm³.

The total energy of the simulation model contains the intramolecular and intermolecular energy. The intramolecular energy includes bend energy, U_θ , and torsional energy, U_φ . The bond length is fixed in this simulation, which is similar with previous works (Supple and

Table 3 Parameters of intramolecular energy used in MD simulations (Supple and Quirke 2004; Supple and Quirke 2005; Yang et al. 2016)

Energy	Octane			
	CH ₃ -CH ₂ -CH ₂		CH ₂ -CH ₂ -CH ₂	
Bend	k_θ	θ (°)	k_θ	θ (°)
	(kcal/mol rad ²)		(kcal/mol rad ²)	
	124.62	114	124.62	114
Torsional	V_1 (kcal/mol)	V_2 (kcal/mol)	V_3 (kcal/mol)	
	0.7078	- 0.1359	1.5696	

Table 4 Parameters of intermolecular energy used in MD simulations (Supple and Quirke 2004, 2005; Yang et al. 2016)

Site	σ (Å)	E (kcal/mol)	Q (e)
Octane			
C in CH ₃	3.75	0.196	-
C in CH ₂	3.95	0.092	-
H in CH ₂ or CH ₃	0	0	-
Graphite			
C	3.4	0.056	-

Quirke 2004, 2005). The bend energy and torsional energy can be calculated as (Van der Ploeg and Berendsen 1982)

$$U_\theta = \frac{1}{2} \sum_i k_\theta (\theta_i - \theta_i^0)^2 \quad (15)$$

$$U_\varphi = \frac{1}{2} \sum_i V_i (1 + \cos i\varphi) \quad (16)$$

where θ_i^0 and φ are the equilibrium angle between two i atoms and the dihedral angle of every four connected i atoms, respectively. Table 3 lists parameters of intramolecular energy used in Eqs. 15–16 (Supple and Quirke 2004, 2005; Yang et al. 2016).

In addition, the van der Waals intermolecular energy in the simulation is described by the Lennard-Jones 12–6 equation (Tee et al. 1966)

$$U_{\text{vdw}}(r) = 4\epsilon_{ij} \left[\left(\frac{\sigma_{ij}}{r} \right)^{12} - \left(\frac{\sigma_{ij}}{r} \right)^6 \right] \quad (17)$$

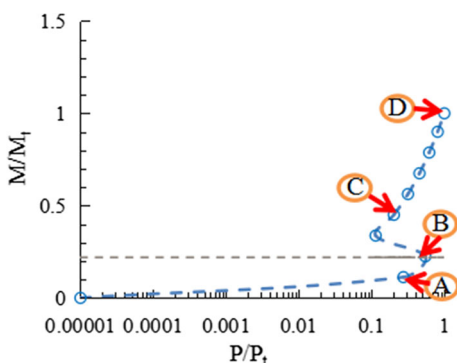
$$\sigma_{ij} = \frac{1}{2} (\sigma_{ii} + \sigma_{jj}) \quad (18)$$

$$\epsilon_{ij} = \sqrt{\epsilon_{ii}\epsilon_{jj}} \quad (19)$$

where $U_{\text{vdw}}(r)$ is the van der Waals energy. ϵ_{ij} , σ_{ij} and r are the potential well, the equilibrium distance, and the distance between atom i and atom j . The force field used in MD simulations is the classical TraPPE force field (Martin and Siepmann 1998), which usually describes interactions of octane/octane molecules and octane/carbon atoms of graphite slit. Details of the simulation are described in previous study (Yang et al. 2016). Table 4 lists parameters of intermolecular energy used in Eqs. 17–19 (Supple and Quirke 2004, 2005; Yang et al. 2016).

We use canonical ensemble (NVT ensemble) for molecular dynamics simulations and Nosé-Hoover thermostat and Verlet integration (Supple and Quirke 2004) to integrate the

Fig. 5 M/M_t versus P/P_t in 2 nm model. Blue dash line and gray dot line represent the imbibition isotherm and phase transition line, respectively. Four characteristic points are discussed in the text. M_t and P_t represent the total imbibed mass and the pressure when the nanopore is fully filled with octane molecules at 298 K, respectively



Newton's equations of motion. The time step of the simulation is 1 fs, and the total simulation time is 300 ps, as previous done (Supple and Quirke 2004, 2005). The Ewald summation is used to calculate long-range Coulomb interaction and the cutoff distance is set to 1.25 nm. The periodic condition is applied in all directions. More details are described in our previous study (Yang et al. 2016).

4 Results

4.1 Vapor–Liquid Equilibrium

In this paper, the conception of vapor state or liquid state represents the fluid which has a vapor or liquid state density. To explain previous imbibition experiments (Habibi et al. 2016), we select the condition of the system is at room temperature and pressure. Since the nanopore is the vacuum at room temperature and pressure, fluid molecules start to imbibe when the nanopore contacts the bulk fluid reservoir. The pressure inside the nanopore increases as fluid molecules imbibe. Therefore, there is a phase transition of imbibed fluid molecules in the nanopore. Considering the phase transition, we use state equations to calculate the pressure of the system, as previously done (Ravikovitch et al. 2001).

Figure 5 shows the normalized imbibed mass, M/M_t , versus the normalized pressure, P/P_t , in 2 nm model calculated by previous study (Ravikovitch et al. 2001). At Point A, fluid molecule starts to imbibe into the nanopore as vapor phase. The pressure inside the nanopore increases as fluid molecules imbibes in. Thus, there is a phase transition as the fluid pressure increases. Considering the phase transition, we use state equations to calculate the pressure of the system, as previously done (Ravikovitch et al. 2001). When the pressure of the imbibed fluid molecules is approaching to Point B, the pressure decreases. This suggests the phase of some fluid molecules transits from vapor to liquid state at Point B. From the first data point to Point B, all fluid molecules imbibe as vapor phase. Due to the fluid/pore attraction, the phase transition starts with adsorbed layers and extents to the pore center. Since molecular interactions are continuous and U-shape (Fig. 4), there is a threshold of driving pressure. Fluid molecules can move, only when the driving pressure is greater than the threshold. These results may be visualized by previous work (Rossi et al. 2004) on water transport in carbon nanotubes. As a result, the distribution of fluid molecules along j -axis is inhomogeneous and not continuous for the whole nanopore. Therefore, we have the assumption c. At Point C, imbibed fluid molecules have transited into liquid phase. The region between Point B and C

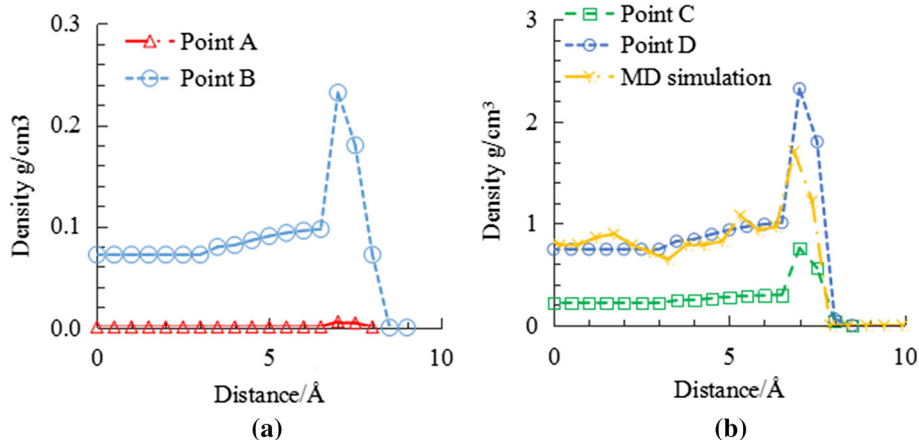


Fig. 6 Octane density profiles versus distances from the slit center in 2 nm nanopore at Point A–B (a) and at Point C–D (b). $x = 0$ represents the slit center

represents the vapor–liquid coexistent region. Within this region, some octane molecules are as vapor phase and others are as liquid phase. The phase transition in this region is reversible.

4.2 Adsorption and Velocity

Figure 6a compares octane density profiles on the cross section of the 2 nm nanopore at Point A and B calculated by Eqs. 1–2. Figure 6b compares density profiles at Point C and D calculated by Eqs. 1–2 and that obtained from simulation, respectively. At Point A, the density of octane molecules near the wall is around 0.0006 g/cm^3 . This result means octane molecules imbibe into nanopore and stay near the pore wall. According to Fig. 4, imbibed octane molecules stay at $2.0 \text{ \AA} \leq x \leq 8.2 \text{ \AA}$, where octane molecules are significantly influenced by the fluid/wall intermolecular interaction.

At Point B, there is a high peak of the density profile ($x \approx 7.1 \text{ \AA}$), which is around 0.22 g/cm^3 , and the density of the center region is around 0.075 g/cm^3 . The density of the region between the center region and the peak is around 0.09 g/cm^3 . Combined with Fig. 4, this peak density is caused by the strong fluid/wall interactions near the wall. In addition, fluid molecules at $5.4 \text{ \AA} \leq x \leq 8.2 \text{ \AA}$ and at $2.0 \text{ \AA} \leq x \leq 5.4 \text{ \AA}$ are defined as the first adsorbed layer and second adsorbed layer, as previously done (Fathi and Akkutlu 2014; Cristancho et al. 2017).

Particularly, octane molecules form adsorbed layers near the wall as vapor phase, and then fill the slit center. As the imbibed molecule increases, the imbibed octane molecules are as liquid phase at Point C. The comparison of Point B and C shows that the phase transition firstly occurs in adsorbed layers and then extends to the slit center. This process is visualized by previous experiments on water transport in 50 nm carbon nanotube (Whitby and Quirke 2007). At Point D, the density profile of MD simulation is similar with that predicted by Eqs. 1–2. The predicted density of the first adsorbed layer and the second layer when $w = 2 \text{ nm}$ are around 2.38 g/cm^3 and 0.80 g/cm^3 , respectively. The density in the center region when $w = 2 \text{ nm}$ is much less than that of adsorbed layers due to the weak fluid/wall interaction. Since the octane molecule is modeled by the hard-sphere model, the impact of the fluid/wall intermolecular interaction on the density oscillation is more obvious than that obtained from

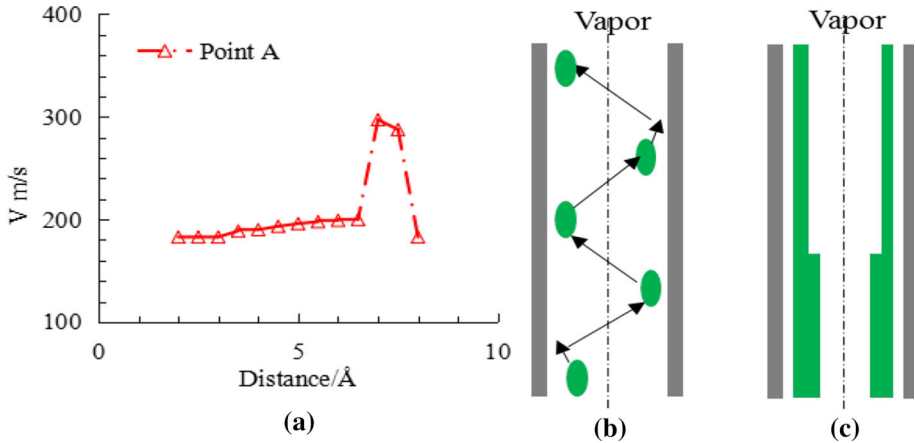


Fig. 7 **a** Velocities predicted by Eq. 13 versus distances from the slit wall, and **b**, **c** schematic illustrations of octane molecules imbibition in the nanopore at Point A. Green spheres and green parts represent single octane molecule and octane molecules, respectively. Gray part represents the wall of the graphite nanopore

MD simulation. Then, densities of the first adsorbed layer calculated by Eq. 1 are higher than those obtained from MD simulation.

Figure 7a shows velocity profiles of imbibed octane molecules at Point A calculated by Eq. 14. Figure 7b, c schematically illustrates the imbibition of the first adsorbed layer and the second adsorbed layer at Point A. In *i*-axis direction, octane molecules form the first adsorbed layer due to the fluid/wall attractive energy. However, octane molecules do not be fixed at the first adsorbed layer place (Fig. 6b). According to Figs. 4 and 7a, octane molecules move fast at about 300 m/s (*j*-axis) due to the strong fluid/wall repulsive energy and the strong driving pressure. Then, octane molecules imbibe into the nanopore at around 200 m/s (*j*-axis) and form the second adsorbed layer (*i*-axis). This fast imbibition of adsorbed layers is also called fast wetting in some references (Supple and Quirke 2004; Gruener et al. 2009). At Point A, both first and second adsorbed layers are vapor phase.

Figure 8 compares velocity profiles obtained from Eqs. 13–14 and MD simulation at Point B and D. After the fast wetting, octane molecules imbibe in the center region of nanopore as vapor phase at Point B. Simulation results at Point B ($t = 20$ ps) show velocities of octane molecules in the center region and second adsorbed layer ($0 \text{ \AA} \leq x \leq 5.4 \text{ \AA}$) fluctuate. Compared to the center region, velocities of adsorbed layers ($5.4 \text{ \AA} \leq x \leq 7.2 \text{ \AA}$) are steadier. In addition, velocity of the center region and the first adsorbed layer are slightly higher than that of the second adsorbed layer. Velocity profiles predicted by the proposed model are similar with simulation results.

When the local pressure (at dl) is above vapor–liquid coexistence pressure (Point C), the liquid fluid is thermodynamically stable. At Point D, predicted velocities of the center region and of the second adsorbed layer are around 48 m/s and 40 m/s, respectively. Velocities of the first adsorbed layer range from 30 to 100 m/s. Due to the strong fluid/wall repulsive energy, the velocity (100 m/s) is extremely high. Velocities of the center region are slightly higher than those of the second adsorbed region. Due to the strong fluid/wall intermolecular interactions, velocities between adsorbed layers and the center region are different. At Point D, M/M_t equals to 1, which means the imbibition is at equilibrium state (liquid phase, $t = 300$ ps). The equilibrium state in this paper exists within short distance (assumption c) and short time (assumption d), which is totally different with that at macroscale. Velocities

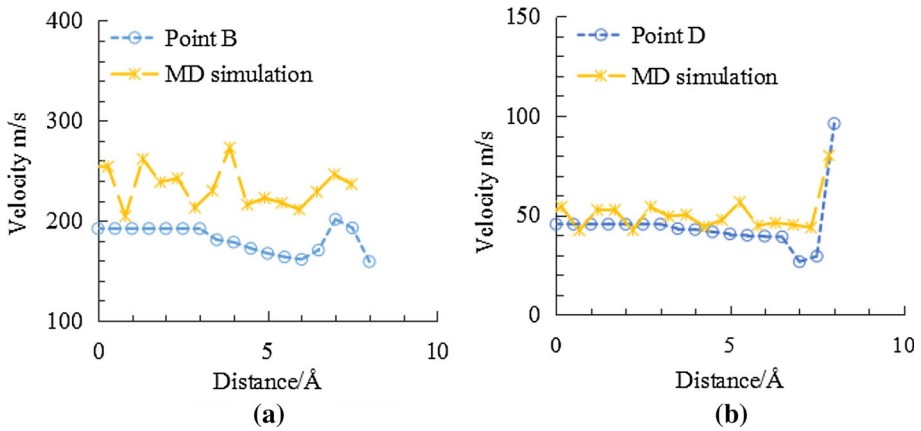


Fig. 8 Velocity profiles at Point B and D obtained from Eqs. 13–14 and MD simulation

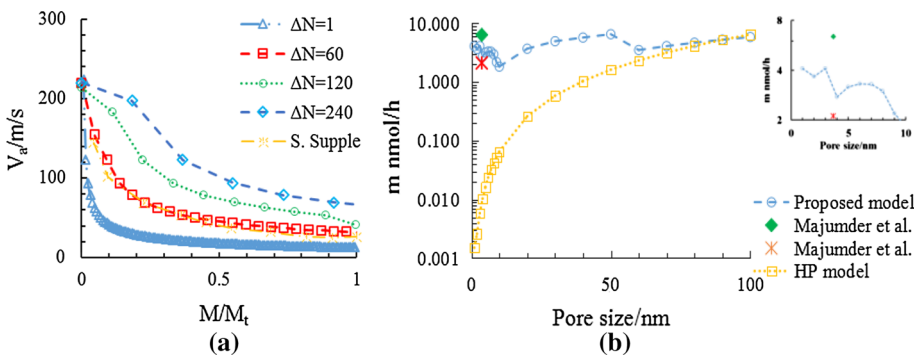


Fig. 9 **a** Mean velocities calculated with different ΔN and simulated by S. Supple (Gruener et al. 2009; Tarazona 1985) versus M/M_t and **b** transport mass of octane molecules calculated by the proposed model and of C9 measured from previous work (Majumder et al. 2005)

predicted by Eqs. 13–14 are similar with those obtained from MD simulation. Compared to Point B, velocities at Point D obtained from the simulation are steadier.

The mean velocity, v_a of imbibed octane molecules at t are calculated as follows

$$v_a = \frac{\int v(x)dx}{w} \tag{20}$$

Figure 9a shows the mean velocity of imbibed octane molecules is a function of M/M_t . As the density of imbibed fluid molecules increases, the velocity of imbibition decreases. Particularly, the velocity of vapor phase decreases fast as the fluid density increases. The impact of the phase transition on fluid imbibition rate is significant. As we know, the contact angle of fluid is hard to define in the nanopores (Whitby and Quirke 2007; Gruener et al. 2009). Thus, the imbibition rate can represent the wettability of nanopores. For different fluid, the wettability and saturated fluid type of the real organic nanopore can be made sure by comparing the imbibition rate predicted by the proposed model. Therefore, the imbibition model in nanopores is significant for reserve estimation, especially for unconventional reservoirs. Due to the phase transition in nanopores, the imbibition rate of LJ fluid in nanopores is significantly higher than that predicted by classical models. These results suggest that

previous experimental results (Lan et al. 2015) of the zero oil contact angle on organic-rich tight rocks, composed of 1–10 nm nanopores, are due to the fast imbibition in organic nanopores.

According to assumption d and Figs. 7 and 8, we know the impact of the time interval when calculating the driving pressure in Eqs. 13–14 on the imbibition rate is significant. Since it is the challenge to get the right time interval, we investigate the impact of such time interval on the imbibition rate by sensitivity analysis in Fig. 9a. The time interval is quantitatively represented by ΔN . ΔN is the interval difference of imbibed fluid number between two time steps in Eq. 6. As ΔN increases, calculated mean velocities increase. Calculated mean velocities of $\Delta N = 60$ are similar with previous studies on decane imbibition into graphite slit (Gruener et al. 2009; Tarazona 1985). These results indicate octane molecules can be displaced in 2 nm organic nanopore when the density difference between fluid reservoir and nanopore is greater than around 0.038 g/cm^3 .

Previous experiments (Majumder et al. 2005b) on imbibition flow of C9 in 3.7 nm carbon nanotubes at 308 K and at atmospheric pressure show the transport mass of C9 measured by MV^{2+} and $Ru-(bipy)_3^{2+}$ are around 6.40 nmol/h and 2.12 nmol/h with 90% confidence. To compare with this experimental result, the transport mass of octane molecules has been calculated and shown in Fig. 9b. The transport mass calculated by the proposed model shows a good agreement with previous experimental results (Majumder et al. 2005b).

4.3 Pore size Sensitivity Analysis

The mean density of imbibed octane molecules is calculated as follows:

$$\rho_a = \frac{\int \rho(x) dx}{w} \quad (21)$$

Since the phase of imbibed fluid significantly affects the fluid velocity, we calculate the velocity of whole imbibition as

$$v_{aw} = \frac{\int_{V+L} v(x) dx}{w} \quad (22)$$

where V and L are vapor and liquid phase of imbibed fluid molecules at distance x , respectively. Figure 10a compares mean densities at equilibrium state predicted by the proposed model and MD simulation. As the pore size increases, mean densities decrease. Mean density of $w = 10 \text{ nm}$ is slightly higher than the bulk density. Compared with MD simulation results, mean densities calculated by proposed model is slightly higher.

Figure 10b compares mean velocities of the whole imbibition and of the equilibrium state. Mean velocity of the whole imbibition is higher than that of the equilibrium state. As the pore size increases, mean velocities of the whole imbibition and equilibrium state decrease. Predicted mean velocities of the whole imbibition is around 10^3 – 10^4 of those calculated by HP equation. In addition, estimated mean velocities of the equilibrium state is around 10^2 – 10^3 of those calculated by HP equation. These velocity results are confirmed by previous study (Whitby and Quirke 2007) on decane and hexane flow in 7 nm carbon nanotubes. When $w = 10 \text{ nm}$, mean velocity at equilibrium state predicted by the proposed model is slightly higher than that calculated by HP equation. These results indicate that the classical imbibition model cannot describe the fluid imbibition in $w \leq 10 \text{ nm}$ organic nanopores. In sum, imbibition rates of fluid octane in less than 10 nm organic nanopores are extremely higher than those predicted by classical imbibition models due to the phase transition and the strong fluid/wall interactions.

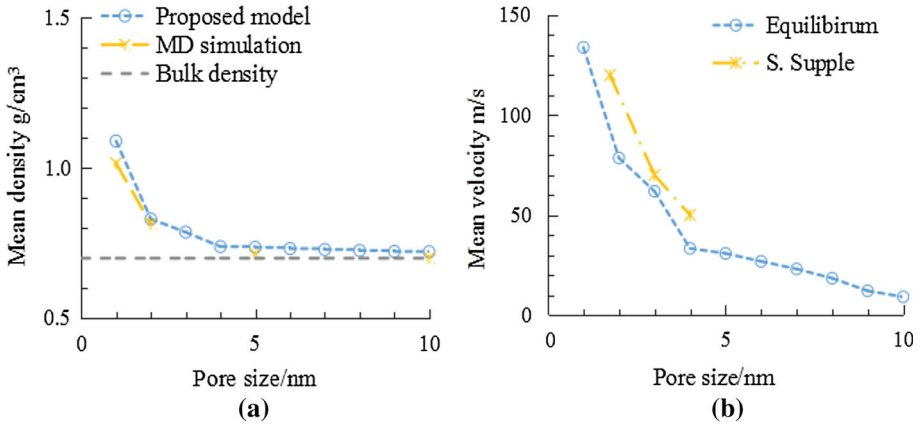


Fig. 10 **a** Mean densities, and **b** mean velocities predicted by proposed model and MD simulations versus pore sizes

Table 5 Parameters of different reservoir pressures and pressure differences

Case	Pressure (MPa)		ΔP (MPa)	T (K)	Bulk density (g cm ⁻³)		Δ Density (g cm ⁻³ dl ⁻¹)
	Initial	Current			Initial	Current	
1	5.72	5.60	0.12	353	0.935	0.931	0.0038
2	11.70	11.56	0.14	353	1.111	1.107	0.0038
3	23.85	23.69	0.16	353	1.419	1.415	0.0038
4	11.70	11.16	0.54	353	1.111	1.096	0.0151
5	23.85	23.21	0.64	353	1.419	1.404	0.0151
6	23.85	23.72	0.135	353	1.419	1.416	0.0031

4.4 Reservoir Condition

To investigate the fluid flow in the organic nanopore of shales, we apply the proposed model on octane molecules transport under reservoir pressures and temperature. According to previous work (Riewchotisakul and Akkutlu 2016) on fluid flow in nanopores of shales, the selected initial pressure and temperature of the shale reservoir are listed in Table 5. The organic nanopore is firstly filled with octane molecules when the pressure of fluid reservoir (Fig. 3) is the initial reservoir pressure. Then, the filled nanopore is placed in the fluid reservoir of current pressure. This process is to mimic the reservoir pressure decrease. Based on analysis above, the density differences are set 0.038 and 0.152 g/cm³. To compare with previous work (Riewchotisakul and Akkutlu 2016), density difference is set as 0.003 g/cm³ (Case 6).

Figure 11 shows calculated velocity profiles of Case 1–5. As the pressure of the system increases, the fluid velocity at the center region decreases and the velocity profile becomes more smooth and steady. Velocities of fluid molecules at high-pressure are steady. In addition, the fluid velocity increases by increasing the pressure difference. Calculated velocities of Case 6 by the proposed model are similar with previous works on methane flow in organic nanopores (Riewchotisakul and Akkutlu 2016) using MD simulations. Based on analysis above, octane molecules in 2 nm organic nanopore of shales will not transport when the

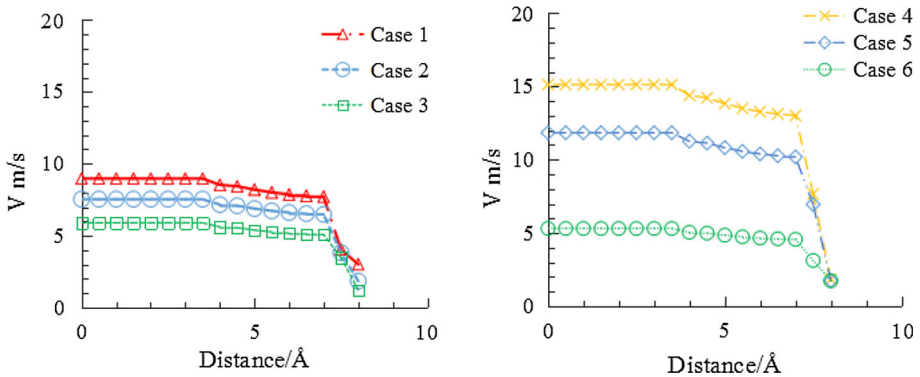


Fig. 11 Velocity profiles of Case 1–5 obtained from Eqs. 13–14

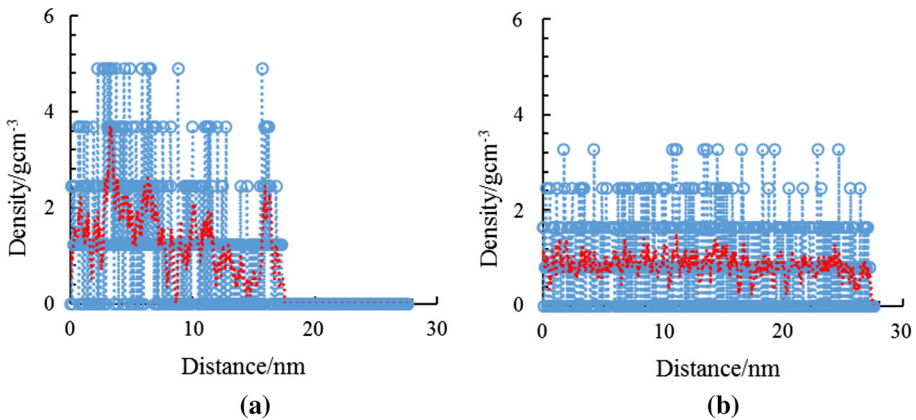


Fig. 12 Imbided fluid densities at imbibition time of 2 ps (a) and 150 ps (b) versus distance along j -axis. Blue circle-dot lines and red solid lines represent simulation data points and fitting lines, respectively

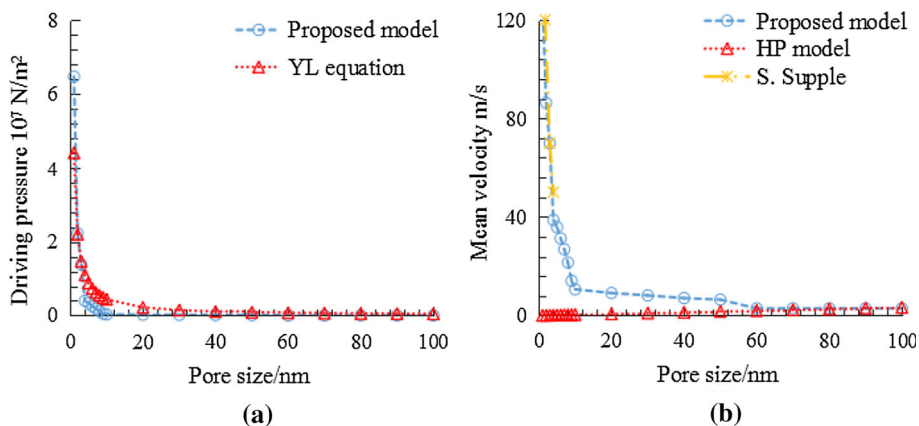
density difference is less than $0.0038 \text{ g}/(\text{cm}^3 \cdot 3 \text{ nm})$. When the density difference is above $0.0038 \text{ g}/(\text{cm}^3 \cdot 3 \text{ nm})$, octane molecules in 2 nm organic nanopores can flow out into the fluid reservoir immediately. These results indicate there is a threshold of driving pressure, fluid can flow only when the driving pressure is above the threshold. Based on our results, such threshold of octane molecules in 2 nm organic nanopore theoretically is 0.12 MPa when the initial reservoir pressure is 5.72 MPa

5 Discussion

It is significant to select the accurate dl to show the fluid phase behavior and transport in the nanopore. Figure 12a, b shows imbided fluid densities are a function of distance along j -axis. Simulation result of 2 ps shows fluid density distribution is inhomogeneous where the distance along j -axis is greater than 5 nm. According to fluid molecule size and assumptions, dl is 3 nm and the selected size of fluid cell to calculate the density and velocity in the proposed model is 1–10 nm (w) \times 5 nm (h) \times 3 nm (dl).

Table 6 Calculated mean velocities at equilibrium state with different α

Pore size (nm)	Average velocities (m/s)			
	$\alpha = 0.002$	$\alpha = 0.01$	$\alpha = 0.1$	$\alpha = 0.5$
1	212.9	212.3	208.6	182.8
2	183.1	182.5	179.4	157.2
5	78.8	78.6	77.2	67.6
10	41.2	41.1	30.4	35.4

**Fig. 13** **a** Driving pressure and **b** mean velocities predicted by proposed model versus pore sizes

Since it is a challenge to get accurate α , we compare mean velocities at equilibrium state with different α , listed in Table 6. Calculated mean velocities of 2 nm models with $\alpha = 0.002$ and $\alpha = 0.5$ are 183 m/s and 157 m/s, respectively. This shows that the impact of α on the mean velocity is not significant.

Figure 13a, b compares driving pressures and mean velocities predicted by the proposed model and classical models. We apply the proposed model on 1–100 nm to investigate the clearly range of the proposed model. Driving pressure of the proposed model is greater than that calculated by YL equation when $1 \leq w \leq 2$ nm. The difference of driving pressure between proposed model and YL equation decreases as the pore size increases. When w is around 40 nm, two model's driving pressure results are the same. The difference of mean velocity between the proposed model and HP model decreases as the pore size increases. When w is around 70 nm, mean velocities of two models are the same. According to previous work (Barrow 1973; Riewchotisakul and Akkutlu 2016) and our results, the pore size for the proposed model for liquid state fluid at room temperature and pressure is less than 50 nm.

6 Conclusions

We developed an analytical model for imbibition of LJ fluid molecules into organic nanopores under the standard and reservoir condition. We applied the proposed model on the imbibition of octane into 1–10 nm graphite slits. In addition, we simulated octane molecules imbibition into 1–10 nm graphite slits to compare with the proposed model. The key results are as follows:

Result 1: Firstly, octane molecules imbibe into the 2 nm graphite nanopore as vapor phase at around 300 m/s and form the first adsorbed layer. Then, octane molecules imbibe as vapor phase at around 200 m/s and form the second adsorbed layer. This process is also called fast wetting (Supple and Quirke 2005). After the fast wetting, octane molecules of the center region imbibe at around 190 m/s and those of the first adsorbed layer imbibe at around 160–200 m/s, respectively.

Result 2: In 2 nm analytical model of octane molecules imbibition, mean velocities of vapor phase are around 180–200 m/s and of liquid phase are around 50–120 m/s, respectively. Velocities decrease significantly as densities of imbibed fluid molecules increase.

Result 3: The threshold of driving pressure for octane in 2 nm organic nanopore is around 0.12 MPa when the initial reservoir pressure is 5.72 MPa. As the reservoir pressure decline increases and initial reservoir pressure decreases, the velocity increases.

Results 1–2 indicate that fluid imbibes fast in 1–10 nm organic nanopores due to the strong fluid/wall intermolecular interactions and the phase transition. Previous experiment (Whitby and Quirke 2007) on decane pressure-driven flow in 7 nm carbon nanotube presented that flow rates are four to five orders of magnitude faster than those predicted by classical models. Previous results (Whitby and Quirke 2007) verify our velocity results predicted by the proposed model and MD simulations. Results 3 suggest a theoretic estimation of recoverable hydrocarbon in organic nanopores of shale reservoir.

In this work, the implication of the proposed model in nanopore network of real shale or coal rocks has not been investigated due to limitations in the acquisition of high-resolution 3D rock images, the lack of compositional analysis of organic nanopores and the absence of the fluid imbibition analytical model in 10–100 nm pores. In the future, we plan to investigate fluid imbibition flow in nanopores of real rock samples.

Acknowledgements The authors thank National Natural Science Foundation of China and National Major Scientific and Technological Special Project (2016ZX05048-003) for funding this study.

Appendix A: Classical DFT

DFT (Tarazona 1985) has been widely employed in describing the capillary adsorption isotherms and predicting density profiles in nanopores, such as slit-shape nanopores (Li et al. 2014). We model the density profiles of a LJ fluid flow in slit-shape nanopore at constant temperature, T . The grand canonical potential, $\Omega(\rho(x))$, of the fluid molecules at x can be described as (Tarazona 1985)

$$\Omega(\rho(x)) = F_{\text{int}}[\rho(x)] - \int_V \rho(x)[\mu - V_{\text{ext}}(x)]dx \quad (\text{A1})$$

where $F_{\text{int}}[\rho(x)]$ is the intrinsic Helmholtz free energy function. $V_{\text{ext}}(x)$ and $\rho(x)$ are the full external potential and the density at x , respectively. μ is the chemical potential of the bulk fluid.

For the excess Helmholtz free energy calculation, we use the hard-sphere model (Tarazona 1985) to calculate the repulsive interactions, $F_{\text{h}}[\rho(x); d]$ and the mean field theory to calculate attractive interactions, $F_{\text{att}}[\rho(x)]$ as:

$$F_{\text{int}}[\rho(x)] = F_{\text{h}}[\rho(x); d] + F_{\text{att}}[\rho(x)] \quad (\text{A2})$$

$$F_h[\rho(x)] = kT \int_V \rho [\ln(\Lambda^3 \rho) - 1] dx + \int_V \rho(x) f_{ex}[\bar{\rho}(x); d] dx \tag{A3}$$

$$F_{att}[\rho(x)] = \frac{1}{2} \iint_V \rho(x)\rho(x')\Phi_{att}(|x - x'|) dx dx' \tag{A4}$$

where Φ_{att} and $\bar{\rho}(x)$ are the fluid/fluid van der Waals attraction potential and smoothed density of an implicit equation, respectively. $f_{ex}[\rho(x); d]$ and k are the excess hard-sphere Helmholtz free energy at x and the Boltzmann constant, respectively. Λ is the thermal de Broglie wavelength. $\rho\sigma^3$ is the reduced density. x' is the distance of fluid molecules to the slit center.

We use the Lennard-Jones 12-6 equation to calculate the fluid/fluid van der Waals interaction potential, Φ_{ff} and the fluid/solid van der Waals interaction potential, Φ_{sf} , as follows (Tarazona 1985)

$$V_{ext}(x) = \phi_{sf}\left(x + \frac{w}{2}\right) + \phi_{sf}\left(\frac{w}{2} - x\right) \tag{A5}$$

$$\Phi_{att}(|x - x'|) = \begin{cases} \Phi_{ff}(|x - x'|), & |x - x'| > r_m \\ -\epsilon_{ff}, & |x - x'| < r_m \end{cases} \tag{A6}$$

$$r_m = 2^{1/6}\sigma_{ff} \tag{A7}$$

$$\Phi_{ff}(x) = 4\epsilon_{ff} \left[\left(\frac{\sigma_{ff}}{x - x'}\right)^{12} - \left(\frac{\sigma_{ff}}{x - x'}\right)^6 \right] \tag{A8}$$

$$\Phi_{sf}\left(x + \frac{w}{2}\right) = 4\epsilon_{sf} \left[\left(\frac{\sigma_{sf}}{x + \frac{w}{2}}\right)^{12} - \left(\frac{\sigma_{sf}}{x + \frac{w}{2}}\right)^6 \right] \tag{A9}$$

where σ_{ff} and σ_{sf} are the minimum of the Lennard-Jones potential (well depth), respectively. ϵ_{ff} and ϵ_{sf} are the equilibrium distance, respectively. r_m is the distance of the minimum Lennard-Jones potential.

We use weight functions $w(x; \rho)$ (Tarazona 1985) to calculate density profiles, which has a power series expansion, as

$$\bar{\rho}(x) = \int_V \bar{\rho}(x)w[|x - x'|; \bar{\rho}(x)] dx \tag{A10}$$

$$w(|x - x'|; \bar{\rho}(x)) = w_0(x - x') + w_1(x - x')\bar{\rho}(x) + w_2(x - x')\bar{\rho}(x)^2 \tag{A11}$$

where w_i is the weighting function factor (Tarazona 1985) ($i = 0, 1, 2$).

Due to the grand canonical potential is minimized,

$$\left[\frac{\partial \Omega(\rho)}{\partial \rho} \right]_{\rho(r)} = 0 \tag{A12}$$

The indeterminate Lagrange multiplier, $\lambda(x)$ (Lastoskie et al. 1993), is introduced to avoid the functional derivative under the integral sign in the Euler equation. The density can be calculated as follows:

$$\ln \rho(x) = \frac{1}{kT} \left(-\mu + V_{ext}(x) + f_{ex}(\bar{\rho}(x)) + \int_V \rho(x')\Phi_{att}(|x - x'|) dx' - kT \int_V \lambda(x')w[|x - x'|; \bar{\rho}(x')] dx' \right) - \ln \Lambda^3 \tag{A13}$$

$$\lambda(x) = \frac{-\rho(x)f'_{\text{ex}}(\bar{\rho}(x))/kT}{\left[1 - \int_V \frac{\partial w[|x-x'|;\bar{\rho}(x)]}{\partial \bar{\rho}(x)} \rho(x') dx'\right]} \quad (\text{A14})$$

where $f_{\text{ex}}[\rho(x);d]$ and Λ are the excess hard-sphere Helmholtz free energy and the thermal de Broglie wavelength, respectively. k and w_i are the Boltzmann constant and normalized weight function (Tarazona 1985), respectively. λ and μ are the Lagrange multiplier and chemical potential of the bulk fluid, respectively.

References

- Barrow, G.M.: Physical Chemistry. McGraw-Hill, New York (1973)
- Cai, J., Yu, B.: A discussion of the effect of tortuosity on the capillary imbibition in porous media. *Transp. Porous Media* **89**(2), 251–263 (2011)
- Cai, J., Perfect, E., Cheng, C.L., Hu, X.: Generalized modeling of spontaneous imbibition based on Hagen–Poiseuille flow in tortuous capillaries with variably shaped apertures. *Langmuir* **30**(18), 5142–5151 (2014)
- Cristancho, D., Akkutlu, I.Y., Wang, Y., Criscenti, L.J.: Shale gas storage in kerogen nanopores with surface heterogeneities. *Appl. Geochem.* **84**, 1–10 (2017)
- Fathi, E., Akkutlu, I.Y.: Multi-component gas transport and adsorption effects during CO₂, injection and enhanced shale gas recovery. *Int. J. Coal Geol.* **123**(2), 52–61 (2014)
- Gruener, S., Hofmann, T., Wallacher, D., Kityk, A.V., Huber, P.: Capillary rise of water in hydrophilic nanopores. *Phys. Rev. E* **79**(6), 067301 (2009)
- Habibi, A., Dehghanpour, H., Binazadeh, M., Bryan, D., Uswak, G.: Advances in understanding wettability of tight oil formations: a Montney case study. *SPE Reserv. Eval. Eng.* **19**(04), 583–603 (2016)
- Hummer, G., Garde, S., García, A.E., Pohorille, A., Pratt, L.R.: An information theory model of hydrophobic interactions. *Proc. Natl. Acad. Sci.* **93**(17), 8951–8955 (1996)
- Jin, Z., Firoozabadi, A.: Flow of methane in shale nanopores at low and high pressure by molecular dynamics simulations. *J. Chem. Phys.* **143**(10), 064705 (2015)
- Jin, Z., Firoozabadi, A.: Phase behavior and flow in shale nanopores from molecular simulations. *Fluid Phase Equilib.* **430**, 156–168 (2016)
- Lan, Q., Dehghanpour, H., Wood, J., Sanei, H.: Wettability of the Montney tight gas formation. *SPE Reserv. Eval. Eng.* **18**, 417–431 (2015)
- Lastoskie, C., Gubbins, K.E., Quirke, N.: Pore size heterogeneity and the carbon slit pore: a density functional theory model. *Langmuir* **9**(10), 2693–2702 (1993)
- Li, Z., Jin, Z., Firoozabadi, A.: Phase behavior and adsorption of pure substances and mixtures and characterization in nanopore structures by density functional theory. *SPE J.* **19**(06), 1–096 (2014)
- Liu, C., Li, Z.: On the validity of the navier-stokes equations for nanoscale liquid flows: the role of channel size. *AIP Adv.* **1**(3), 977 (2011)
- Majumder, M., Chopra, N., Andrews, R., Hinds, B.J.: Enhanced flow in carbon nanotubes. *Nature* **438**(7064), 44 (2005a)
- Majumder, M., Chopra, N., Hinds, B.J.: Effect of tip functionalization on transport through vertically oriented carbon nanotube membranes. *J. Am. Chem. Soc.* **127**(25), 9062 (2005b)
- Martin, M.G., Siepmann, J.I.: Transferable potentials for phase equilibria. 1. United-atom description of n-alkanes. *J. Phys. Chem. B* **102**(14), 2569–2577 (1998)
- McQuarrie, D.A.: Statistical Mechanics, p. 3. Harper & Row, New York (1976)
- Qin, X., Yuan, Q., Zhao, Y., Xie, S., Liu, Z.: Measurement of the rate of water translocation through carbon nanotubes. *Nano Lett.* **11**(5), 2173–2177 (2011)
- Ravikovitch, P.I., Vishnyakov, A., Neimark, A.V.: Density functional theories and molecular simulations of adsorption and phase transitions in nanopores. *Phys. Rev. E Stat. Nonlinear Soft Matter Phys.* **64**(1), 011602 (2001)
- Riewchotisakul, S., Akkutlu, I.Y.: Adsorption-enhanced transport of hydrocarbons in organic nanopores. *SPE J.* **21**(06), 1–960 (2016)
- Rossi, M.P., Ye, H., Gogotsi, Y., Babu, S., Ndungu, P., Bradley, J.C.: Environmental scanning electron microscopy study of water in carbon nanopipes. *Nano Lett.* **4**(5), 989–993 (2004)
- Rowlinson, B.S., Widom, B.: Molecular Theory of Capillarity. Clarendon Press, Oxford (1982)

- Saif, T., Lin, Q., Singh, K., Bijeljic, B., Blunt, M.J.: Dynamic imaging of oil shale pyrolysis using synchrotron X-ray microtomography. *Geophys. Res. Lett.* **43**(13), 6799–6807 (2016)
- Sokhan, V.P., Nicholson, D., Quirke, N.: Fluid flow in nanopores: an examination of hydrodynamic boundary conditions. *J. Chem. Phys.* **115**(8), 3878–3887 (2001)
- Supple, S., Quirke, N.: Molecular dynamics of transient oil flows in nanopores I: imbibition speeds for single wall carbon nanotubes. *J. Chem. Phys.* **121**(17), 8571–8579 (2004)
- Supple, S., Quirke, N.: Molecular dynamics of transient oil flows in nanopores. II: Density profiles and molecular structure for decane in carbon nanotubes. *J. Chem. Phys.* **122**(10), 273 (2005)
- Tarazona, P.: Free-energy density functional for hard spheres. *Phys. Rev. A* **31**(4), 2672 (1985)
- Tee, L.S., Gotoh, S., Stewart, W.E.: Molecular parameters for normal fluids. Lennard-Jones 12-6 Potential. *Ind. Eng. Chem. Fundam.* **5**(3), 356–363 (1966)
- Van der Ploeg, P., Berendsen, H.J.C.: Molecular dynamics simulation of a bilayer membrane. *J. Chem. Phys.* **76**(6), 3271–3276 (1982)
- Wang, L., Neeves, K., Yin, X., Ozkan, E.: Experimental study and modeling of the effect of pore size distribution on hydrocarbon phase behavior in nanopores. In: *SPE Annual Technical Conference and Exhibition*. Society of Petroleum Engineers (2014)
- Wang, S., Javadpour, F., Feng, Q.: Molecular dynamics simulations of oil transport through inorganic nanopores in shale. *Fuel* **171**, 74–86 (2016)
- Whitby, M., Quirke, N.: Fluid flow in carbon nanotubes and nanopipes. *Nat. Nanotechnol.* **2**(2), 87–94 (2007)
- Yang, S., Dehghanpour, H., Binazadeh, M., Dong, P.: A molecular dynamics explanation for fast imbibition of oil in organic tight rocks. *Fuel* **190**, 409–419 (2016)
- Yassin, M.R., Dehghanpour, H., Wood, J., Lan, Q.: A theory for relative permeability of unconventional rocks with dual-wettability pore network. *SPE J.* **21**, 1–970 (2016)
- Zeng, M., Mi, J., Zhong, C.: Wetting behavior of spherical nanoparticles at a vapor-liquid interface: a density functional theory study. *Phys. Chem. Chem. Phys.* **13**(9), 3932–3941 (2011)

Publisher's Note Springer Nature remains neutral with regard to jurisdictional claims in published maps and institutional affiliations.